# Vapor-liquid equilibrium, thermodynamic properties, process simulation and economic evaluation of CPME and methanol system

Joshi, Kedar; Parsana, Vyomesh M.; Khirsariya, Priyank; Ramdin, Mahinder; Vlugt, Thijs J.H.

**DOI**
10.1002/aic.18877

**Publication date**
2025

**Document Version**
Final published version

**Published in**
AIChE Journal

Received: 15 November 2024 | Revised: 16 February 2025 | Accepted: 22 April 2025

DOI: 10.1002/aic.18877

AIChE JOURNAL

RESEARCH ARTICLE

Thermodynamics and Molecular-scale Phenomena

# Vapor-liquid equilibrium, thermodynamic properties, process simulation and economic evaluation of CPME and methanol system

Kedar Joshi[1] | Vyomesh M. Parsana[2] | Priyank Khirsariya[2] | Mahinder Ramdin[3] | Thijs J. H. Vlugt[3]

[1]Department of Chemical Engineering, Faculty of Engineering and Technology, Marwadi University, Rajkot, Gujarat, India

[2]Chemical Engineering Department, V.V.P. Engineering College, Gujarat Technological University, Rajkot, Gujarat, India

[3]Engineering Thermodynamics, Process and Energy Department, Faculty of Mechanical, Maritime and Materials Engineering, Delft University of Technology, Delft, The Netherlands

**Correspondence**
Vyomesh M. Parsana, Chemical Engineering Department, V.V.P. Engineering College, Gujarat Technological University, Rajkot 360005, Gujarat, India.
Email: vm_parsana@yahoo.com

**Funding information**
Gujarat Technological University, Grant/Award Number: GTU/IQAC/RPS-MRP/Sanction Letter/2024/3064

## Abstract

Cyclopentyl methyl ether (CPME) is a promising green solvent due to its eco-friendly properties; it is produced by adding methanol (MeOH) to cyclopentene. Separation of the resulting product mixture containing CPME and MeOH is critical, and it requires vapor-liquid equilibrium (VLE) data. In this work, isobaric VLE data were measured experimentally using an ebulliometer in a 60.0–101.3 kPa pressure range for a binary system of CPME + MeOH. VLE data were modeled using excess Gibbs ($G^E$) energy-based models such as Wilson, NRTL, and UNIQUAC. The formation of an azeotrope was analyzed. Flash point, surface tension, Gibbs adsorption, and thickness of surface layer were estimated using the Wilson model, which can help in determining molecule interaction and overall behavior of the system. Atmospheric and high-pressure distillation columns were designed using Aspen Plus to study the separation of CPME + MeOH, and an economic evaluation of the same was carried out.

**KEYWORDS**
azeotrope, cyclopentyl methyl ether, economic analysis, excess properties, methanol, process simulation, surface properties, VLE

## 1 | INTRODUCTION

Various conventional ethereal solvents are available for use in organic synthesis, such as diethyl ether (Et2O), tetrahydrofuran (THF), dimethoxyethane (DME), and dioxane. Often, these solvents have demerits of a lower boiling point, peroxide (PO) formation, and solubility in water (which makes their recovery challenging). One alternative to conventional solvents is methyl tert-butyl ether (MTBE), but it has a low flash point, a high solubility in water, instability under acidic conditions, and is not eco-friendly. The second alternative is 2-methyltetrahydrofuran (2-MeTHF), which is promising as a green solvent, but its major limitation is PO formation and very high solubility in water.

To overcome the above-mentioned limitations and challenges, Watanabe et al. explored the use of cyclopentyl methyl ether (CPME).[1] This solvent is hydrophobic in nature (making it easy to dry), less susceptible to PO formation, has relatively high stability under acidic and basic conditions, and features a low latent heat of vaporization and narrow explosion range.

Several methods are available in the literature for the synthesis of CPME: (1) Methylation of cyclopentanol using dimethyl sulfate, (2) two-step reaction of cyclopentanol using sodium hydroxide and methyl iodide, and (3) addition of methanol (MeOH) to cyclopentene. Method 1 uses dimethyl sulfate, while method 2 incorporates the use of methyl iodide, both of which are carcinogenic/mutagenic to humans. The most promising synthesis route is method 3, as it is more viable for industries due to its high yield. Reaction time for this reaction is 6–8 h involving methanol, cyclopentene and an acidic ion-exchange resin and particular temperature and pressure.[1–6] To ensure a high level of purity for CPME, it is imperative to separate CPME + MeOH after the reaction.

**TABLE 1** CAS number, suppliers, and mass fraction purity of chemicals used.

| Chemicals | CAS number | Supplier | Purity (%) |
|---|---|---|---|
| Cyclopentyl methyl ether (CPME) | 5614-37-9 | LOBA Chemie Pvt. Ltd. | 99.9 |
| Methanol (MeOH) | 67-56-1 | LOBA Chemie Pvt. Ltd. | 99.5 |
| Acetone | 67-64-1 | LOBA Chemie Pvt. Ltd. | 99.5 |

**TABLE 2** Properties for CPME and MeOH.

| Chemicals | Cyclopentyl methyl ether (CPME) | Methanol (MeOH) |
|---|---|---|
| Molecular structure | 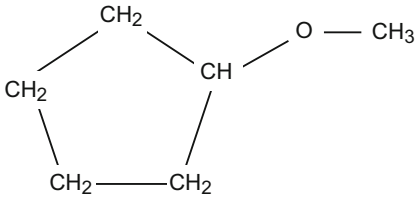 | 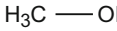 |
| nD[a] (293.15 K) | 1.41896/1.4189[35] | 1.32604/1.3260[35] |
| Molecular weight (g/mol) | 100.16[35] | 32.05[35] |
| Density (g/cm$^3$ at 293.15 K) | 0.86[35] | 0.79[36] |
| Flash point (K) | 274.15[35] | 285.15[35] |
| Surface tension (N/m) (293.15 K) | 0.02517[35] | 0.02230[35] |
| Kinematic viscosity (m$^2$/s) (293.15 K) | $6.3953 \times 10^{-7}$[35] | $7.4684 \times 10^{-7}$[35] |

[a]Experimental value of this work (with $u(T) = 0.5$ K)/literature value.

To design and optimize the synthesis method for CPME accurately, thermodynamic properties of CPME + MeOH are needed, which are not available in the literature to the best of our knowledge, except for isothermal VLE data reported by Jeong et al. at 313.15–353.15 K.[7] The separation column (distillation column) design requires isobaric VLE data of CPME + MeOH. In this work, isobaric VLE data for the said binary system of CPME + MeOH were determined at 60.0–101.3 kPa. The experimental VLE data were correlated using excess Gibbs ($G^E$) energy-based models of Wilson, NRTL, and UNIQUAC.

Apart from the need for VLE data to design a separation/distillation column, the flash point of a binary mixture is crucial in safety and fire hazard studies. In the absence of experimental data, flash points can be predicted using $G^E$-based models.[8] Flash point is a property of the liquid, and $G^E$-based models are accurate in representing the non-ideality of liquid mixtures. In this work, flash points of the CPME + MeOH binary mixture were estimated at 101.3 kPa.

Liquid surface properties such as surface tension, relative Gibbs adsorption, and thickness of surface layer can help in understanding interaction in binary mixtures. Furthermore, they can help in achieving more thermodynamically efficient evaporation, condensation, droplet formation, and heat transfer during distillation. These properties can be estimated using $G^E$-based models.[9] We have estimated these properties for the CPME + MeOH binary mixture at 298.15 K.

Distillation columns were simulated at 101.3, 506.5, and 1013.0 kPa for the separation of CPME + MeOH binary mixture using Aspen Plus V14 software, and economics were evaluated for the same.

**TABLE 3** Deviation in pure component vapor pressure from literature value[a].

| $T$/K | $P_{EXP}$/kPa | $P_{LIT}$/kPa | $(P_{EXP} - P_{LIT}$[b]$)/P_{LIT}$/% |
|---|---|---|---|
| CPME | | | |
| 378.75 | 101.3 | 100.1 | 1.24 |
| 375.05 | 90.0 | 89.9 | 0.09 |
| 370.85 | 80.0 | 79.4 | 0.71 |
| 366.05 | 70.0 | 68.7 | 1.90 |
| 361.85 | 60.0 | 60.3 | −0.49 |
| MeOH | | | |
| 339.15 | 101.3 | 100.1 | 1.19 |
| 336.05 | 90.0 | 88.6 | 1.59 |
| 333.05 | 80.0 | 78.5 | 1.89 |
| 329.95 | 70.0 | 69.1 | 1.25 |
| 326.45 | 60.0 | 59.7 | 0.53 |

[a]Standard uncertainties: $u(T) = 0.5$ K, $u(P) = 0.133$ kPa.
[b]Literature vapor pressure from Parsana and Parikh[37] for CPME and Camacho et al.[38] for MeOH.

This article is structured as follows. In the experimental measurement section, the details of the VLE measurement have been provided. In the thermodynamic modeling section, VLE calculations and properties estimated using VLE data are discussed. In the results and discussion section, experimental and estimated properties are discussed along with results from process simulation and their economic evaluation. In conclusion, the findings of this work have been summarized.

## 2 | EXPERIMENTAL MEASUREMENT

### 2.1 | Materials/chemicals

All the chemicals used in the experimentation were obtained from LOBA Chemie Pvt. Ltd. and they were used without further purification (Table 1). Their purity was checked by measuring their refractive indices, and they were in accordance with the literature data. These data, along with common properties of chemicals, are given in Table 2.

### 2.2 | Reliability check of experimental setup

Consistency tests, often based on the Gibbs-Duhem equation, are prevalent in literature, but they are typically limited to *PTxy* data.[10] The modified ebulliometer employed in this research generated *PTx* data.[11] Wisniak[12] suggests that conducting a consistency test for isobaric VLE data involves determining the heat of mixing at the bubble point for various concentrations, a task that is notably challenging. Therefore, the reliability of the VLE data was assessed by comparing experimental and literature vapor pressures. The results, detailed in Table 3, reveal vapor pressure deviations ranging from −0.49% to 1.24% for CPME, and 0.53% to 1.19% for MeOH. A visual representation is provided in Figure 1. Moreover, Figure 2 offers a visual comparison between experimental vapor pressures and those calculated using Antoine correlation.

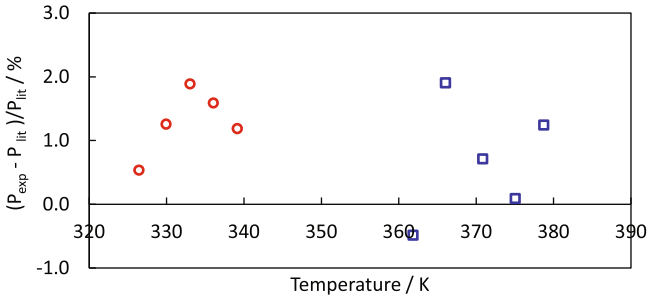


**FIGURE 1** Residual plot of vapor pressure versus temperature for CPME (square) and MeOH (circle).

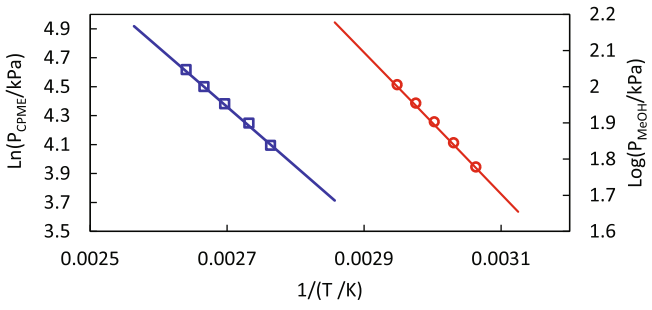


**FIGURE 2** Comparison of pure component vapor pressure: Antoine equation (lines) and experiments (symbols) for CPME (blue) and MeOH (red).

### 2.3 | Experimental measurement of isobaric VLE data

Isobaric VLE data were measured by a modified ebulliometer in a pressure range of 60.0–101.3 kPa. Initially, 60 mL of a binary mixture with a known composition was charged into the ebulliometer. A variable metallic belt heater then heats the mixture and initiates the formation of a vapor phase. At the top section, a double-coil condenser was provided to condense the vapor using chiller water as the cooling medium. When vaporization and condensation rates were equal, equilibrium was considered to be achieved. The temperature of the mixture was measured using a Pt-100 sensor. Simultaneously, the drop count of condensate also indicated equilibrium. Once the drop count and temperature were constant for 10 min, the indicated temperature was reported as the equilibrium bubble point of the mixture. The approximate time to reach the equilibrium state was 30–40 min. Vacuum pressure was applied to the apparatus using a vacuum pump, and its magnitude was controlled via a valve. To maintain stability under atmospheric pressure, a glass ballast tank was used to connect a vacuum pump to the apparatus. Pressure during the experiment was measured by a mercury-filled U-tube manometer, which was connected to the other end of the ebulliometer. Once the bubble point at atmospheric pressure was reported, the vacuum was applied to the system using a vacuum pump. After each run of the experiment, the setup was thoroughly cleaned using acetone and then through a nitrogen purge to prevent contamination. A detailed description and experimental setup, along with its schematic diagram, is provided in our previous work.[13]

### 2.4 | Determination of liquid phase composition at equilibrium

Refractive index was used to determine the liquid phase composition. After each experimentation, the concentration of the mixture was

**TABLE 4** Antoine parameters for CPME and MeOH.

| Component | *A* | *B* | *C* | Normal boiling point[a] | Reference |
|---|---|---|---|---|---|
| CPME[b] | 15.0255 | 3798.52 | −14.2 | 378.75/379.19 | Parsana and Parikh[37] |
| MeOH[c] | 5.15853 | 1569.613 | −34.846 | 339.15/339.46 | Camacho et al.[38] |

[a]Experimental value of this work (with $u(T) = 0.5$ K)/literature value.
[b]$lnP_i^{sat}/\text{kPa} = A - [B/(T/\text{K} + C)]$.
[c]$\log_{10}P_i^{sat}/\text{bar} = A - [B/(T/\text{K} + C)]$.

**TABLE 5** UNIQUAC parameters: *R*(volume) and *Q*(surface area).[39]

| Compound (i) | Group | Main group No. | Secondary group No. (k) | $v_k^{(i)}$ | $R_k$ | $r_i$ | $Q_k$ | $q_i$ |
|---|---|---|---|---|---|---|---|---|
| CPME | $CH_2$ | 1 | 2 | 4 | 0.6744 | 4.2835 | 0.54 | 3.476 |
| | CH | 1 | 3 | 1 | 0.4469 | | 0.228 | |
| | $CH_3O$ | 13 | 24 | 1 | 1.145 | | 1.088 | |
| MeOH | $CH_3OH$ | 6 | 15 | 1 | 1.4311 | 1.4311 | 1.432 | 1.432 |

*Note*: $v_k^{(i)}$: Presence of group *k* in component *i*, $r_i = \sum_k v_k^{(i)} R_k$, $q_i = \sum_k v_k^{(i)} Q_k$.

**TABLE 6** Experimental isobaric *Tx* data for CPME + MeOH at[a].

| 101.3 kPa | | 90.0 kPa | | 80.0 kPa | | 70.0 kPa | | 60.0 kPa | |
|---|---|---|---|---|---|---|---|---|---|
| $x_{CPME}$ | $T_{EXP}$/K | $x_{CPME}$ | $T_{EXP}$/K | $x_{CPME}$ | $T_{EXP}$/K | $x_{CPME}$ | $T_{EXP}$/K | $x_{CPME}$ | $T_{EXP}$/K |
| 0.000 | 339.15 | 0.000 | 336.05 | 0.000 | 333.05 | 0.000 | 329.95 | 0.000 | 326.45 |
| 0.031 | 339.05 | 0.031 | 335.95 | 0.031 | 332.95 | 0.031 | 329.75 | 0.031 | 325.95 |
| 0.065 | 338.95 | 0.065 | 335.95 | 0.065 | 332.75 | 0.065 | 329.45 | 0.065 | 325.85 |
| 0.104 | 339.05 | 0.104 | 335.95 | 0.104 | 332.85 | 0.104 | 329.75 | 0.104 | 325.95 |
| 0.148 | 339.25 | 0.148 | 336.15 | 0.148 | 332.95 | 0.148 | 329.85 | 0.148 | 325.95 |
| 0.199 | 339.65 | 0.199 | 336.35 | 0.199 | 333.35 | 0.199 | 330.15 | 0.199 | 326.25 |
| 0.258 | 340.05 | 0.258 | 336.75 | 0.258 | 333.65 | 0.258 | 330.25 | 0.258 | 326.55 |
| 0.328 | 340.45 | 0.328 | 337.25 | 0.328 | 334.05 | 0.328 | 330.75 | 0.328 | 326.95 |
| 0.411 | 341.35 | 0.411 | 337.95 | 0.411 | 334.85 | 0.411 | 331.35 | 0.411 | 327.65 |
| 0.511 | 342.25 | 0.511 | 339.25 | 0.511 | 335.75 | 0.511 | 332.45 | 0.511 | 328.55 |
| 0.635 | 344.15 | 0.635 | 340.75 | 0.635 | 337.75 | 0.635 | 334.35 | 0.635 | 329.45 |
| 0.725 | 347.05 | 0.725 | 343.45 | 0.725 | 339.95 | 0.725 | 336.55 | 0.725 | 332.15 |
| 0.793 | 349.45 | 0.793 | 346.05 | 0.793 | 342.65 | 0.793 | 339.25 | 0.793 | 334.65 |
| 0.869 | 355.25 | 0.869 | 351.55 | 0.869 | 347.75 | 0.869 | 343.85 | 0.869 | 339.85 |
| 0.910 | 360.15 | 0.910 | 356.55 | 0.910 | 351.95 | 0.910 | 348.25 | 0.910 | 344.15 |
| 0.954 | 367.55 | 0.954 | 362.75 | 0.954 | 358.95 | 0.954 | 356.25 | 0.954 | 350.65 |
| 1.000 | 378.75 | 1.000 | 375.05 | 1.000 | 370.85 | 1.000 | 366.05 | 1.000 | 361.85 |

[a]Standard uncertainties: $u(T) = 0.5$ K, $u(P) = 0.133$ kPa and $u(x_1) = 0.001$.

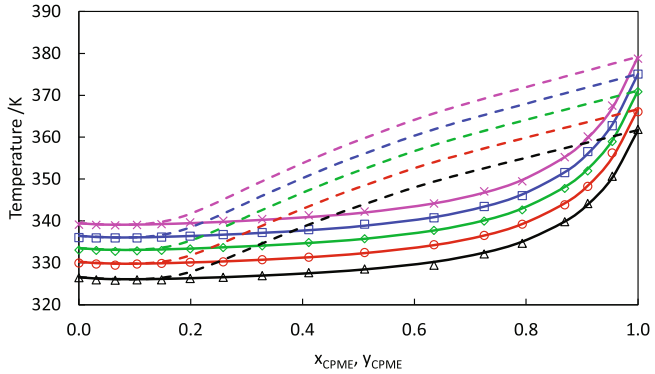


**FIGURE 3** Comparison of experimental bubble points (symbols), Wilson bubble points (solid lines) and Wilson dew points (dashed lines) for CPME + MeOH at different pressures: 101.3 kPa (pink), 90.0 kPa (blue), 80.0 kPa (green), 70.0 kPa (red), and 60.0 kPa (black).

measured using a 5-digit automatic digital refractometer RFM-950 supplied by LABMAN. The measurement range of it was 1.30000–1.70000 with an accuracy of ± 0.00002. A calibration curve was prepared to determine the liquid phase composition: $RI_{mix} = 0.09279 V_{frac,CPME} + 1.32607$ with $R^2 = 0.99998$.

## 3 | THERMODYNAMIC MODELING

### 3.1 | Modified Raoult's law

Experimental VLE data generated in this work were modeled using the $\gamma - \Phi$ correlation as shown in Equation (1).

$$y_i \Phi_i P = x_i \gamma_i P_i^{sat}. \quad (1)$$

Where, $y_i$ is vapor phase mole fraction, $\Phi_i$ is fugacity coefficient, *P* is total pressure, $x_i$ is liquid phase mole fraction, $\gamma_i$ is activity coefficient and $P_i^{sat}$ is vapor pressure of component i. As the experiments were carried out in a pressure range of 60.0–101.3 kPa, a reasonable assumption of fugacity coefficient to be unity was considered ($\Phi_i = 1$). Vapor pressures of both components were correlated using the Antoine equation (constants and equation used for them are reported in Table 4).

### 3.2 | Calculation of activity coefficients using $G^E$-based models

The VLE data obtained from experiments are discrete. They can not be used in modeling distillation columns and/or finding an accurate azeotropic point for the binary system. Therefore, VLE data were correlated using excess Gibbs ($G^E$) energy based models of Wilson,[14] NRTL[15] and UNIQUAC.[16] Wilson model incorporates molar volume, NRTL model performs better when used for electrolytes or non-homogeneous systems, and the UNIQUAC model includes area and volume parameters of the involved groups in binary mixtures. However, in our previous experience,[13,17–21] there was no significant quantifiable difference in their ability to fit VLE data. In this work, the above-mentioned three models were used for VLE correlation, and the Wilson model was used to calculate other properties.

Experimental bubble point ($Tx$) at isobaric conditions were taken as input to $G^E$-based models along with initial guess of binary interaction parameters (BIPs) of the model, and total pressure was calculated using $P_i^{cal} = \sum x_i \gamma_i P_i^{sat}$ equation. Antoine constants reported in Table 4 were used to obtain vapor pressure at the corresponding temperature, and activity coefficients were calculated using $G^E$-based models as a function of temperature ($T$) and liquid phase composition ($x$). Then,

**TABLE 7** BIPs and AADs.

| Model | BIPs /(J/mol) | | AAD (P) | AAD (T) |
|---|---|---|---|---|
| Wilson | $\Delta\lambda_{12}$ | $\Delta\lambda_{21}$ | 0.63 | 0.21 |
| | 600.34 | 4350.54 | | |
| NRTL[a] | $\Delta g_{12}$ | $\Delta g_{21}$ | 0.73 | 0.24 |
| | 785.20 | 3698.49 | | |
| UNIQUAC | $\Delta u_{12}$ | $\Delta u_{21}$ | 0.69 | 0.23 |
| | 3063.63 | −177.97 | | |

[a] $\alpha_{12} = 0.30$.

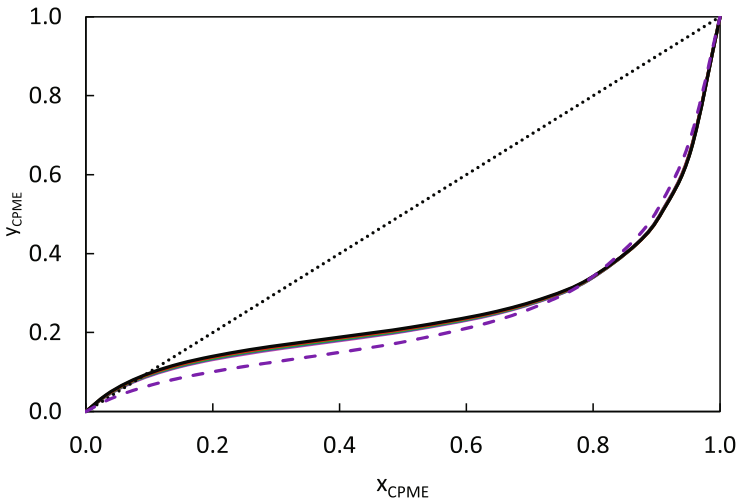


(A) entire concentration range

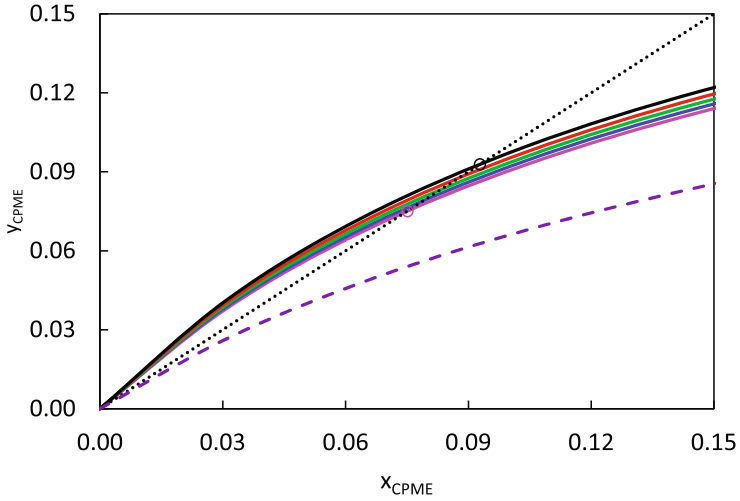


(B) zoomed between $x_1$=0.00 to 0.15

**FIGURE 4** Comparison of equilibrium liquid and vapor phase composition calculated from Wilson model for CPME + MeOH at different pressures: 101.3 kPa (pink), 90.0 kPa (blue), 80.0 kPa (green), 70.0 kPa (red), 60.0 kPa (black), and 1013.0 kPa (dashed line). (a) entire concentration range, (b) zoomed between $x_1$ = 0.00 to 0.15.

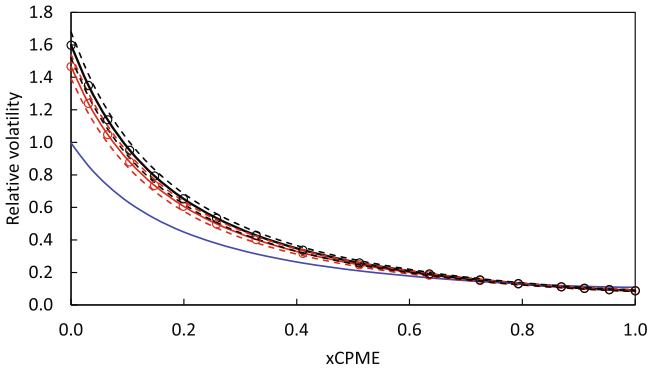


(A) entire concentration range

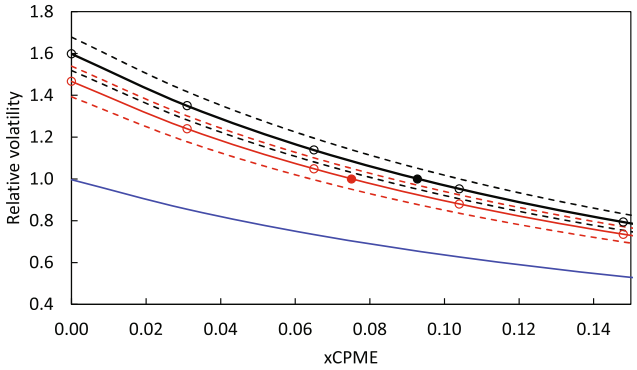


(B) zoomed between $x_1$=0.00 to 0.15

**FIGURE 5** Comparison between experimental relative volatility (circle), Wilson relative volatility (continuous line) with ±5% error line (dashed lines) and relative volatility at azeotropic composition (filled circle) at different pressures: 101.3 kPa (red), 60.0 kPa (black), and 1013.0 kPa (blue). (a) entire concentration range, (b) zoomed between $x_1 = 0.00$ to 0.15.

the difference in experimental pressure and calculated pressure was evaluated, and eventually average absolute deviation (AAD) was calculated using Equation (2).

$$\mathrm{AAD}(P) = \sum_{i}^{n} |P_i^{\mathrm{exp}} - P_i^{\mathrm{cal}}|/n. \quad (2)$$

BIPs were obtained via regression. For this, AAD(*P*) was considered as a minimization function and BIPs as variables in the first set of optimization calculations. In the second step, temperatures were regressed by keeping the same AAD(*P*) as the minimization function. Similar to AAD(*P*), the deviation in temperature was also calculated as per Equation (3)

$$\mathrm{AAD}(T) = \sum_{i}^{n} |T_i^{\mathrm{exp}} - T_i^{\mathrm{cal}}|/n. \quad (3)$$

These regression calculations were carried out in an MS Excel spreadsheet.

### 3.3 | Flash point, excess properties and viscosity calculations

The flash point of the binary mixture was calculated using the Wilson model at a pressure of 101.3 kPa. Initially, bubble point temperatures of the mixture at corresponding compositions were taken as an initial guess and regressed by taking Equation (4) as the objective function.

$$1 = \sum_{i=1}^{n} \frac{x_i \gamma_i P_i^{\mathrm{sat}}}{P_{i,fp}^{sat}}. \quad (4)$$

Where $x_i$ is liquid phase mole fraction of component i, $\gamma_i$ is activity coefficient of component i, $P_i^{sat}$ is vapor pressure of component i at

| Pressure/kPa | $x_{CPME} = y_{CPME}$ | $T_{mix,az}$/K | $T_{b,CPME}$/K | $T_{b,MeOH}$/K |
|---|---|---|---|---|
| 60.0 | 0.093 | 326.08 | 361.69 | 326.58 |
| 70.0 | 0.088 | 329.80 | 366.67 | 330.25 |
| 80.0 | 0.083 | 333.09 | 371.09 | 333.51 |
| 90.0 | 0.079 | 336.06 | 375.08 | 336.45 |
| 101.3 | 0.075 | 339.10 | 379.18 | 339.45 |
| 202.6 | 0.052 | 358.16 | 405.22 | 358.35 |
| 303.9 | 0.039 | 370.42 | 422.26 | 370.53 |
| 405.2 | 0.029 | 379.68 | 435.27 | 379.75 |
| 506.5 | 0.022 | 387.21 | 445.95 | 387.26 |
| 607.8 | 0.016 | 393.61 | 455.09 | 393.63 |
| 709.1 | 0.011 | 399.20 | 463.12 | 399.21 |
| 810.4 | 0.007 | 404.18 | 470.32 | 404.18 |
| 911.7 | 0.003 | 408.68 | 476.86 | 408.68 |
| 1013.0 | No azeotrope | No azeotrope | 482.87 | 412.80 |
| 1114.3 | No azeotrope | No azeotrope | 488.45 | 416.61 |

**TABLE 8** Variation in azeotropic composition ($x_{CPME} = y_{CPME}$), azeotropic temperature ($T_{mix,az}$) and pure component boiling point ($T_b$) with pressure for CPME + MeOH system[a].

[a]Standard uncertainties: $u(T) = 0.5$ K, $u(P) = 0.133$ kPa and $u(x_1) = 0.001$.

**TABLE 9** Properties estimated from Wilson model at 298.15 K for CPME + MeOH[a].

| $x_{CPME}$ | $G^E$ (J mol$^{-1}$) | $H^E$ (J mol$^{-1}$) | $S^E$ (J mol$^{-1}$ K$^{-1}$) | $C_P^E$ (J mol$^{-1}$ K$^{-1}$) | $T_{FP}$ (K) | $\sigma$ (N m$^{-1}$) | $\Gamma_{2,1} \times 10^6$ (mol m$^{-2}$) | $t$ (Å) | $v \times 10^7$ (m$^2$ s$^{-1}$) |
|---|---|---|---|---|---|---|---|---|---|
| 0.00 | 0.0000 | 0.0000 | 0.0000 | 0.0000 | 285.15 | 0.0223 | – | – | 7.4684 |
| 0.05 | 205.3231 | 130.3884 | −0.2513 | 0.6069 | 279.24 | 0.0225 | 1.8031 | 1.1225 | 6.5279 |
| 0.10 | 378.3221 | 247.3318 | −0.4393 | 1.1517 | 276.52 | 0.0227 | 1.8560 | 1.1345 | 5.8345 |
| 0.15 | 522.9446 | 352.5393 | −0.5715 | 1.6293 | 275.03 | 0.0228 | 1.8934 | 1.1440 | 5.3157 |
| 0.20 | 642.1273 | 446.9097 | −0.6548 | 2.0363 | 274.12 | 0.0229 | 1.9186 | 1.1520 | 4.9250 |
| 0.25 | 738.1078 | 530.8260 | −0.6952 | 2.3697 | 273.53 | 0.0230 | 1.9331 | 1.1592 | 4.6316 |
| 0.30 | 812.6190 | 604.3150 | −0.6987 | 2.6277 | 273.11 | 0.0232 | 1.9377 | 1.1662 | 4.4148 |
| 0.35 | 867.0183 | 667.1352 | −0.6704 | 2.8084 | 272.81 | 0.0233 | 1.9323 | 1.1734 | 4.2604 |
| 0.40 | 902.3732 | 718.8243 | −0.6156 | 2.9107 | 272.57 | 0.0234 | 1.9156 | 1.1814 | 4.1586 |
| 0.45 | 919.5221 | 758.7233 | −0.5393 | 2.9343 | 272.39 | 0.0235 | 1.8861 | 1.1912 | 4.1026 |
| 0.50 | 919.1165 | 785.9835 | −0.4465 | 2.8796 | 272.24 | 0.0236 | 1.8396 | 1.2037 | 4.0883 |
| 0.55 | 901.6517 | 799.5613 | −0.3424 | 2.7485 | 272.11 | 0.0238 | 1.7713 | 1.2222 | 4.1130 |
| 0.60 | 867.4881 | 798.2038 | −0.2324 | 2.5442 | 272.02 | 0.0240 | 1.6685 | 1.2495 | 4.1759 |
| 0.65 | 816.8668 | 780.4242 | −0.1222 | 2.2726 | 271.95 | 0.0241 | 1.5168 | 1.2974 | 4.2773 |
| 0.70 | 749.9201 | 744.4676 | −0.0183 | 1.9425 | 271.91 | 0.0244 | 1.2881 | 1.3860 | 4.4189 |
| 0.75 | 666.6775 | 688.2651 | 0.0724 | 1.5668 | 271.93 | 0.0246 | 0.9646 | 1.5438 | 4.6037 |
| 0.80 | 567.0690 | 609.3744 | 0.1419 | 1.1644 | 272.00 | 0.0247 | 0.6031 | 1.7194 | 4.8361 |
| 0.85 | 450.9251 | 504.9023 | 0.1810 | 0.7615 | 272.18 | 0.0249 | 0.3262 | 1.8285 | 5.1222 |
| 0.90 | 317.9731 | 371.4060 | 0.1792 | 0.3953 | 272.52 | 0.0250 | 0.1604 | 1.9354 | 5.4700 |
| 0.95 | 167.8316 | 204.7625 | 0.1239 | 0.1175 | 273.12 | 0.0251 | 0.0666 | 2.2318 | 5.8899 |
| 1.00 | 0.0000 | 0.0000 | 0.0000 | 0.0000 | 274.15 | 0.0252 | – | – | 6.3953 |

[a]Relative standard uncertainties: $u_r(G^E) = 0.0046$, $u_r(H^E) = 0.0052$, $u_r(S^E) = 0.0237$, $u_r(C_P^E) = 0.0077$, $u_r(T_{FP}) = 0.000042$, $u(\sigma) = 0.0002$, $u(\Gamma_{2,1}) = 0.0316$, $u(t) = 0.0287$, and $u(v) = 0.0012$.

mixture flash point temperature, and $P_{i,fp}^{sat}$ is vapor pressure of component i at flash point temperature of pure component (reported in Table 2).

Excess Gibbs energy ($G^E$), excess enthalpy ($H^E$), excess entropy ($S^E$) and excess heat capacity ($C_P^E$) were calculated using Equations (5) to (8) at 298.15 K.

$$G^E = RT\sum_i x_i \ln\gamma_i, \tag{5}$$

$$H^E = -RT^2\left[\frac{\partial\left(\frac{G^E}{RT}\right)}{\partial T}\right]_{P,x} = x_1x_2\left[\frac{\Lambda_{12}\Delta\lambda_{12}}{x_1+x_2\Lambda_{12}} + \frac{\Lambda_{21}\Delta\lambda_{21}}{x_2+x_1\Lambda_{21}}\right], \tag{6}$$

$$S^E = \frac{H^E - G^E}{T}, \tag{7}$$

$$C_P^E = \left[\frac{\partial H^E}{\partial T}\right]_{P,x} = \frac{x_1x_2}{RT^2}\left[\frac{x_1\Lambda_{12}\Delta\lambda_{12}^2}{(x_1+x_2\Lambda_{12})^2} + \frac{x_2\Lambda_{21}\Delta\lambda_{21}^2}{(x_2+x_1\Lambda_{21})^2}\right]. \tag{8}$$

Kinematic viscosity of liquid mixture is given by Eyring equation[22,23]

$$\ln(vM) = \sum_{i=1}^{NC} x_i \ln(v_iM_i) + \frac{G^{*,E}}{RT}. \tag{9}$$

Where, $v$ is kinematic viscosity of mixture, $M$ is molecular weight of mixture, $x_i$ is mole fraction of component i, $v_i$ is kinematic viscosity of pure component i, $M_i$ is molecular weight of pure component i, $G^{*,E}$ is excess free energy at activated condition. $G^{*,E}$ is related to excess Gibbs energy ($G^E$) by following equation:

$$G^{*E} = kG^E. \tag{10}$$

Where $k$ is known as the Eyring constant. Novak proposed Modified Eyring equation[24] with $k = -1$.

$$\ln(vM) = \sum_{i=1}^{NC} x_i \ln(v_iM_i) - \frac{G^E}{RT}. \tag{11}$$

We have used the excess Gibbs energy from the Wilson model.

### 3.4 | Surface tension, relative Gibbs adsorption and thickness of surface layer

The estimation of surface properties presents a significant computational challenge. The methodology put forth by Sprow and Prausnitz[25]

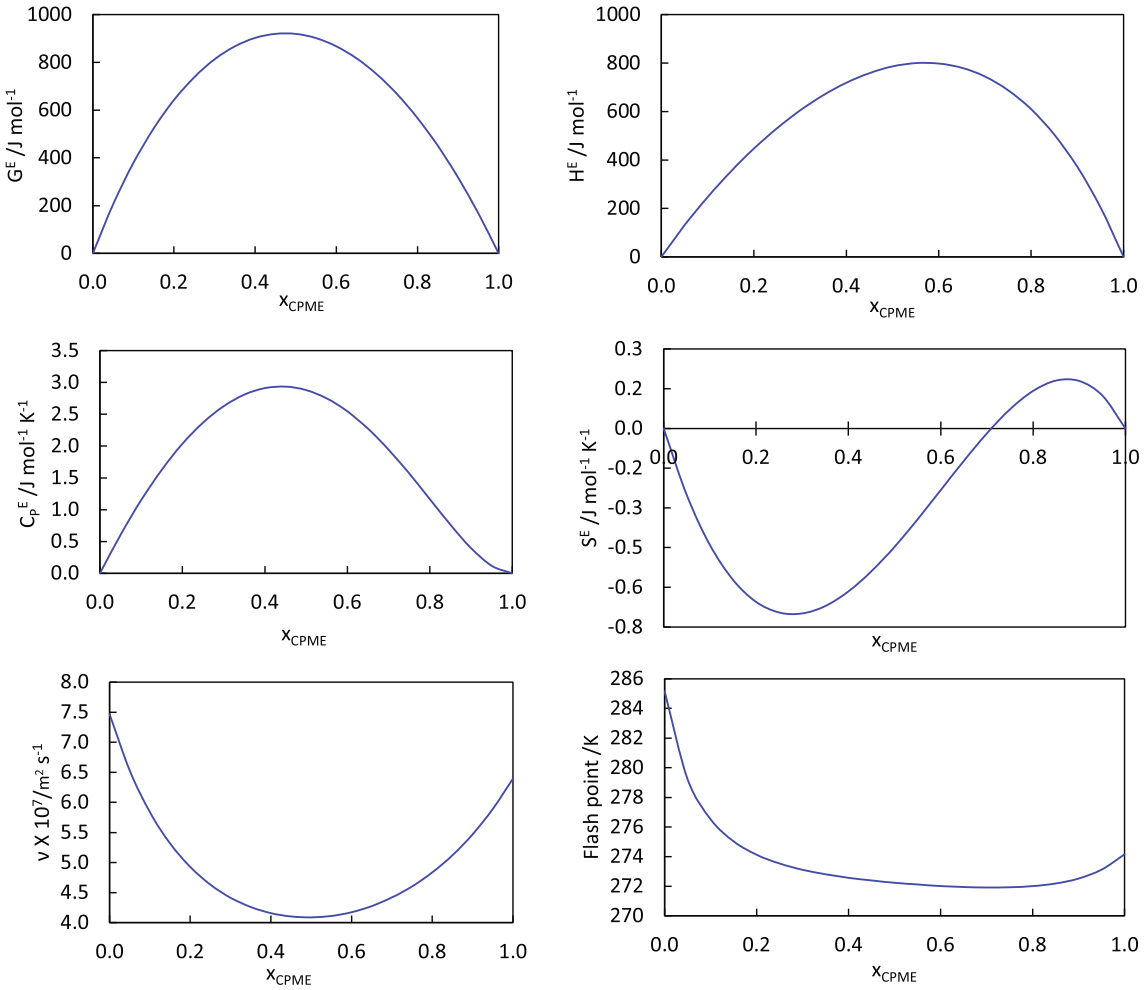


**FIGURE 6** Excess properties, kinematic viscosity and flash point (at 101.3 kPa) calculated from Wilson model for CPME + MeOH at 298.15 K.

has been extensively utilized in conjunction with activity coefficient correlations.[9,26,27]

Prediction of surface properties involves the assumption of treating the surface as a separate thermodynamic phase, as the compositional structure and intermolecular interactions in the surface and bulk of the liquid mixture are different. Based on this assumption, Sprow and Prausnitz[25] proposed following Equation (12) for calculation of surface tension.

$$\sigma = \sigma_i + \frac{RT}{A_i} \ln \frac{x_i^s \gamma_i^s}{x_i^b \gamma_i^b}. \tag{12}$$

Where, $\sigma$ is surface tension of mixture, $\sigma_i$ is surface tension of pure component i, $R$ is universal gas constant, $T$ is temperature, $A_i$ is molar surface area of component i, $x_i$ is liquid phase mole fraction of component i, and $\gamma_i$ is activity coefficient of component i. Superscript $s$ and $b$ represent the surface layer and the liquid bulk phase, respectively. Equation (12) involves liquid phase non-ideality in terms of $\gamma_i$, which was correlated using the Wilson model in this work.

Molar surface area was calculated using an approach suggested by Rasmussen.[28] This approach uses the UNIQUAC area parameter. Equation (13) was used for this calculation:

$$A_i = 2.5 \times 10^9 \sum_k v_{k,i} Q_k. \tag{13}$$

Where $v_{k,j}$ is the presence of group $k$ in component i, $Q_k$ is the van der Waals surface area parameter of group $k$ (reported in Table 5).

Surface tension was obtained by initially guess of $x_i^s$ as $x_i^b$, then $x_i^s$ was regressed by considering Equation (14) as objective function.

$$\sigma_{mix(from\ component\ 1)} - \sigma_{mix(from\ component\ 2)} = 0. \tag{14}$$

Where, $\sigma_{mix(from\ component\ 1)}$ and $\sigma_{mix(from\ component\ 2)}$ are surface tension of mixture calculated as shown in Equations (15) and (16).

$$\sigma_{mix(from\ component\ 1)} = \sigma_1 + \frac{RT}{A_1} \ln \frac{x_1^s \gamma_1^s}{x_1^b \gamma_1^b}, \tag{15}$$

$$\sigma_{mix(from\ component\ 2)} = \sigma_2 + \frac{RT}{A_2} \ln \frac{x_2^s \gamma_2^s}{x_2^b \gamma_2^b}. \quad (16)$$

The relative Gibbs adsorption ($\Gamma_{2,1}$) was calculated using Equation (17).

$$\Gamma_{2,1} = -\frac{1}{RT}\left(\frac{\partial \sigma}{\partial \ln(x_2\gamma_2)}\right). \quad (17)$$

The thickness of surface layer ($t$) was calculated using Equation (18).

$$t = -\frac{1}{RT}\left(\frac{\partial \sigma}{\partial \ln a_2}\right)\left(\frac{\phi_2^s}{v_2} - \frac{\phi_1^s}{v_1}\frac{x_2^b}{x_1^b}\right)^{-1}. \quad (18)$$

The volume fraction in the surface layer and bulk phase was calculated using Equation (19) and (20) respectively.

$$\phi_2^s = \frac{n_2^s v_2}{n_1^s v_1 + n_2^s v_2} = 1 - \phi_1^s, \quad (19)$$

$$\phi_2^b = \frac{n_2^b v_2}{n_1^b v_1 + n_2^b v_2} = 1 - \phi_1^b. \quad (20)$$

Where $n_i$ is the number of moles of component $i$ and $v_i$ is the molar volume of component i. Superscript $s$ and $b$ represent the surface layer and the liquid bulk phase, respectively.

A variety of methods for estimating surface properties can be found in the literature. The primary goal of this research is to determine the surface properties of the CPME + MeOH binary mixture, thereby providing initial estimates that can serve as a basis for further investigations or simulations of analogous systems. Nevertheless, the Sprow and Prausnitz model is not ideal for the accurate evaluation of interfacial properties of intricate mixtures, as it is more applicable to simpler mixtures where regular solution theory can effectively model surface phase behavior.

For enhanced accuracy in predicting surface properties, the Peng–Robinson equation of state,[29] along with a modified Huron–Vidal mixing rule[30] and square gradient theory, as demonstrated by Mejia et al.,[31–33] represents a viable alternative. Furthermore, Kleinheins et al.[34] have explored several other methodologies, and many of them require experimental surface property data.

## 4 | RESULTS AND DISCUSSION

### 4.1 | VLE Measurement and related properties

VLE data were measured for the binary system of CPME + MeOH at isobaric pressures of 101.3, 90.0, 80.0, 70.0, and 60.0 kPa. These data are reported in Table 6 in the form of $P$ (kPa), $T$ (K) and $x_1$ (liquid phase composition at equilibrium).

A comparison between experimental VLE data and modeling results obtained from Wilson in the form of a $Txy$ plot is given in Figure 3. Similar behavior was observed in NRTL and UNIQUAC models. The bubble point of the mixture decreases to the extent of a minimum at the azeotropic point near the diluted end of CPME ($x_{CPME}$ = 0.075–0.093) and then increases till the pure component boiling point of CPME. This nature is similar in all models. As pressure increases from 60.0 to 101.3 kPa, the azeotropic temperature increases and the azeotropic composition decreases.

The performance of $G^E$-based models is reported in Table 7, where binary interaction parameters (BIPs) and average absolute deviations (AADs) in pressure and temperature are reported for each model. The order of best-fitting to least-fitting of models is *Wilson > UNIQUAC > NRTL*. The Wilson model performed best in fitting VLE data with AAD ($P$) = 0.63 and AAD ($T$) = 0.21. Therefore, it was used for a detailed study of azeotrope formation, excess properties, flash point, and surface properties.

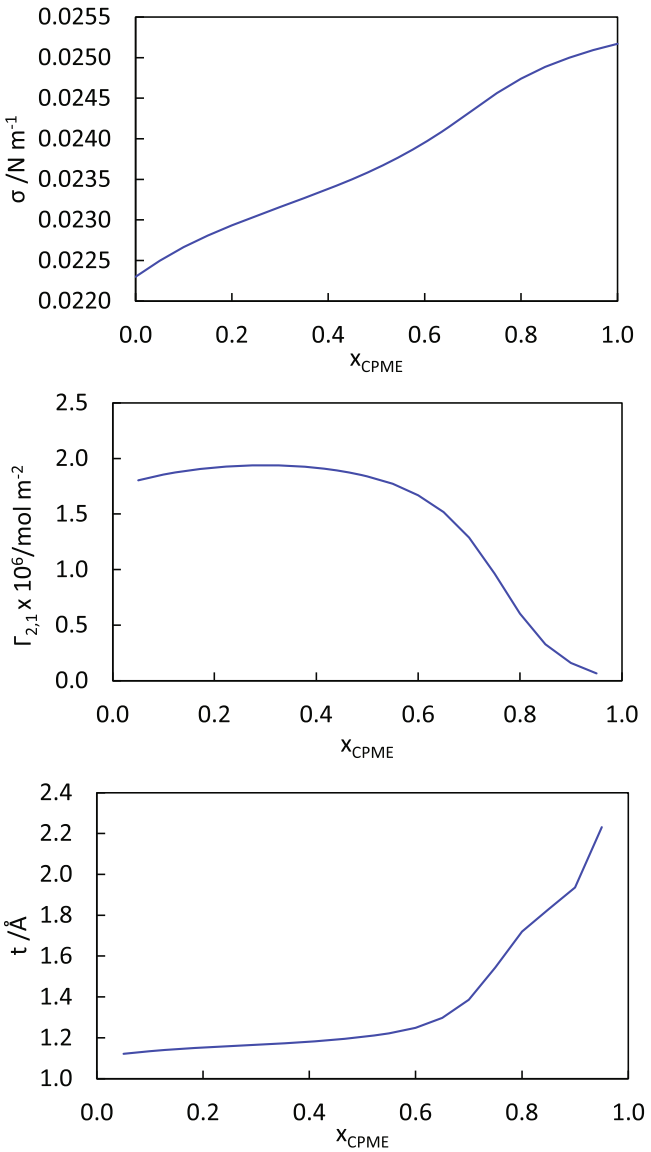


**FIGURE 7** Surface tension, relative Gibbs adsorption and thickness of surface layer (at 298.15 K) calculated from Wilson model for CPME + MeOH.

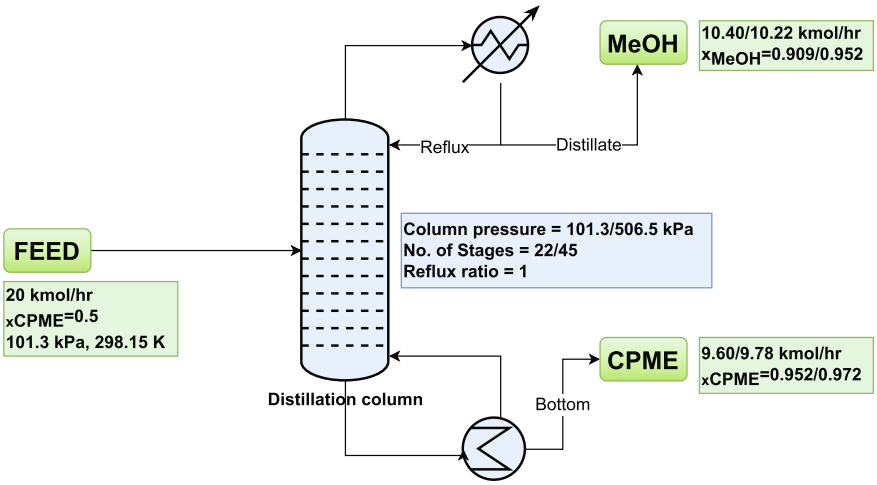


(A) Case 1 and 2

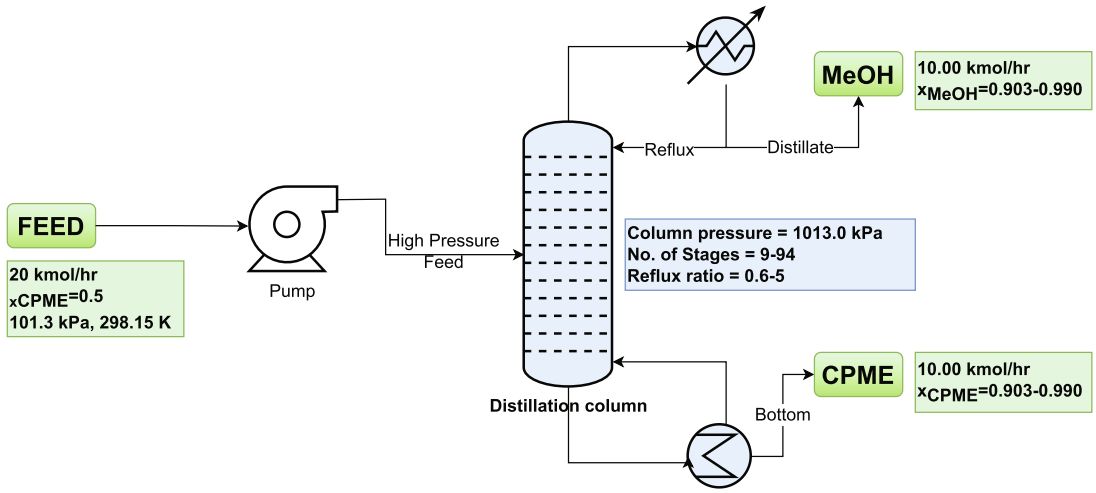


(B) Case 3–7

**FIGURE 8** Process simulation flowsheet for different cases. (a) Cases 1 and 2, (b) Cases 3–7.

As *Txy* and *xy* plot clearly indicate the formation of an azeotrope, the phenomenon was further investigated using the best-fitting Wilson model. With the increase in pressure from 60.0 to 101.0 kPa, the azeotrope shifts towards the pure end of MeOH (as shown in Figure 4). Relative volatilities at 101.3 and 60.0 kPa are represented in Figure 5. Azeotropic compositions, azeotropic and boiling temperatures with change in pressures are reported in Table 8. Azeotropic behavior is examined comprehensively by determining azeotropic composition at different pressures ranging from 60.0 to 1114.3 kPa. As pressure increases, the azeotropic composition decreases, and at 1013.0 kPa, there is no azeotrope. The values are reported in Table 8.

Excess Gibbs energy ($G^E$), excess enthalpy ($H^E$), excess entropy ($S^E$) and excess heat capacity ($C_p^E$), flash point ($T_{FP}$), surface tension ($\sigma$), relative Gibbs Adsorption ($\Gamma_{2,1}$), thickness of surface layer ($t$) and kinematic viscosity ($v$) obtained using the Wilson model are reported in Table 9. Graphical representation of excess properties (at 298.15 K) is given in Figure 6. $G^E$ and $H^E$ were observed to be positive in the entire concentration range, indicating positive deviation from ideality. Particularly, $G^E > 0$ stipulates repulsion between molecules and $H^E > 0$ indicates endothermic mixing. $S^E$ was observed to be negative within the range of $x_{CPME} = 0$–$0.655$ (less than ideal disorder upon mixing), while in the rest of the range it was positive (more than ideal disorder upon mixing). $G^E$ plot attained a maximum value near $x_1 = 0.450$, while $H^E$ peaked at a value near $x_1 = 0.550$. The positive maximum value of $S^E$ achieved near $x_1 = 0.850$, while the negative was achieved at $x_1 = 0.300$. $C_p^E$ was positive for the entire concentration range, indicating a higher requirement of heat than the ideal requirement for a change in temperature, and it peaked near $x_1 = 0.450$. kinematic

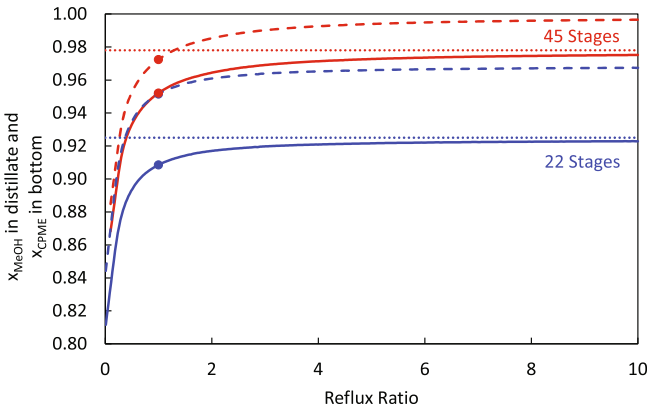


**FIGURE 9** Relation between purity of MeOH in distillate (continuous lines), purity of CPME in bottom (dashed lines) with reflux ratio for Case 1 (blue) and Case 2 (red); actual reflux used in simulation (circle); azeotropic composition limitation (round dot lines).

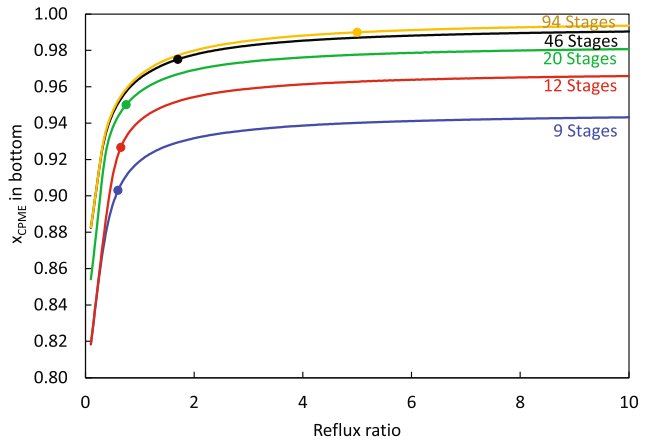


**FIGURE 10** Relation between purity of CPME in bottom (lines) with reflux ratio for Case 3 (blue), Case 4 (red), Case 5 (green), Case 6 (black), and Case 7 (yellow); actual reflux used in simulation (circle).

viscosity of mixture decreases with increase in CPME concentration and reaches minimum in the vicinity of equal molar concentration (Figure 6).

Flash points of CPME + MeOH binary mixture evaluated using Wilson model at 101.3 kPa are given in Figure 6. Flash point of mixtures decreases with an increase in concentration of CPME and attains a minimum value near $x_1 = 0.700$, and then it increases slightly and reaches up to the pure component flash point.

Surface tension, relative Gibbs adsorption, and thickness of surface layer (at 298.15 K) are represented graphically in Figure 7. Surface tension increases with increases in concentration of CPME. Relative Gibbs adsorption increases gradually with concentration of CPME and achieves a maximum value at $x_{CPME} = 0.300$, then it decreases gradually till $x_{CPME} = 0.600$, after this point (near pure end of CPME) it decreases rapidly. The thickness of the surface layer increases gradually with the concentration of CPME till $x_{CPME} = 0.600$, then the increment is more rapid as it reaches its maximum value near the pure end of CPME. This phenomenon indicates a greater tendency towards mixing and no adsorption near the pure end of CPME.

**TABLE 11** Plant parameters.

| Plant lifetime (year) | 20 |
|---|---|
| Plant location | US |
| Currency | USD |
| Feed processing capacity (kmol/hr) | 20 |

**TABLE 12** Cost of utilities.[40]

| Utilities | Price | Unit |
|---|---|---|
| Electricity | 18.72 | $/GJ |
| Cooling water | 0.378 | $/GJ |
| High-pressure steam | 5.66 | $/GJ |

**TABLE 10** Case-wise simulation parameter details.

| Parameters | Case | 1 | 2 | 3 | 4 | 5 | 6 | 7 |
|---|---|---|---|---|---|---|---|---|
| Feed | Flowrate (kmol/hr) | 20 | 20 | 20 | 20 | 20 | 20 | 20 |
| | $x_{MeOH}$ | 0.5 | 0.5 | 0.5 | 0.5 | 0.5 | 0.5 | 0.5 |
| | $x_{CPME}$ | 0.5 | 0.5 | 0.5 | 0.5 | 0.5 | 0.5 | 0.5 |
| Column variable | Pressure (kPa) | 101.3 | 506.5 | 1013.0 | 1013.0 | 1013.0 | 1013.0 | 1013.0 |
| | Stages | 22 | 45 | 9 | 12 | 20 | 46 | 94 |
| | Feed stage | 14 | 36 | 8 | 11 | 18 | 39 | 82 |
| | Reflux ratio | 1.00 | 1.00 | 0.60 | 0.65 | 0.75 | 1.70 | 5.00 |
| Distillate | Flowrate (kmol/hr) | 10.40 | 10.22 | 10.00 | 10.00 | 10.00 | 10.00 | 10.00 |
| | $x_{MeOH}$ | 0.909 | 0.952 | 0.903 | 0.927 | 0.950 | 0.975 | 0.990 |
| | $x_{CPME}$ | 0.091 | 0.048 | 0.097 | 0.073 | 0.050 | 0.025 | 0.010 |
| Bottom | Flowrate (kmol/hr) | 9.60 | 9.78 | 10.00 | 10.00 | 10.00 | 10.00 | 10.00 |
| | $x_{MeOH}$ | 0.048 | 0.028 | 0.097 | 0.073 | 0.050 | 0.025 | 0.010 |
| | $x_{CPME}$ | 0.952 | 0.972 | 0.903 | 0.927 | 0.950 | 0.975 | 0.990 |

(Continues)

**TABLE 10** (Continued)

| Parameters | Case | 1 | 2 | 3 | 4 | 5 | 6 | 7 |
|---|---|---|---|---|---|---|---|---|
| Duty | Condensor duty (MW) | −0.5100 | −0.1781 | −0.1282 | −0.1324 | −0.1407 | −0.2174 | −0.4838 |
| | Reboiler duty (MW) | 0.5570 | 0.2847 | 0.2585 | 0.2662 | 0.2789 | 0.3618 | 0.6328 |

**TABLE 13** Case-wise normalized cost.

| Case | 1 | 2 | 3 | 4 | 5 | 6 | 7 |
|---|---|---|---|---|---|---|---|
| Total capital cost ($/kmol CPME) | 1.39 | 1.51 | 1.38 | 1.36 | 1.35 | 1.49 | 2.58 |
| Total operating cost ($/kmol CPME) | 12.71 | 12.78 | 12.74 | 12.46 | 12.25 | 12.70 | 17.83 |
| Total cost($/kmol CPME) | 14.10 | 14.29 | 14.13 | 13.81 | 13.60 | 14.20 | 20.41 |

## 4.2 | Process simulation and economic evaluation

The binary mixture of CPME + MeOH was separated using a distillation column. The simulation studies were conducted using Aspen Plus V14. The distillation column was designed at three different pressures: 101.3, 506.5, and 1013.0 kPa. Azeotrope formation was observed near the pure end of MeOH (at the lower side of the *Txy* plot), hence the limitation of purity was observed for the bottom product of distillation. The first two pressures had limitations of 92.5% and 97.8% purity of MeOH in the distillate, respectively, due to azeotrope formation (see Table 8). However, the high pressure of 1013.0 kPa did not exhibit any azeotrope formation. Therefore, a total of seven case studies were evaluated: The first and second case studies were conducted at pressures of 101.3 and 506.5 kPa to achieve the highest possible purities, while the third to seventh case studies were evaluated at 1013.0 kPa to achieve purities of 90.0%, 92.5%, 95%, 97%, and 99.0%. The flowsheet of the process simulation can be found in Figure 8.

The Wilson model performed best in terms of VLE data fitting. Therefore, the Wilson model was used in Aspen Plus by taking input from Table 7 and Antoine constant from Table 4. Feed flow rate of 20 kmol/hr and equimolar composition were taken as input for all the cases. For Case 1, the feed was directly fed into the distillation column, while for cases 2 and 3–7, a pump was used to achieve high pressures of 506.5 and 1013.0 kPa, respectively. The RADFRAC module was used to simulate a distillation column. Stage efficiency was taken as 75% in all cases. Once the number of stages was fixed, purity was achieved by adjusting the reflux ratio.

Figure 9 illustrates the change in composition with reflux ratio for a given stage configuration in cases 1 and 2. Despite employing a very high reflux ratio, achieving a near-azeotrope composition was extremely challenging. In the atmospheric pressure distillation column (Case 1), 22 stages were required, whereas the high-pressure column at 505.5 kPa (Case 2) required 45 stages. Additionally, Case 2 was capable of achieving a high purity of the bottom stream. Figure 10 demonstrates the same relationship between reflux ratio and composition for cases 3–7. In this scenario, it was assumed that the distillate and bottom product flow rates remain equal, as the split between the rectification and stripping sections of the column was considered to be the same. As a

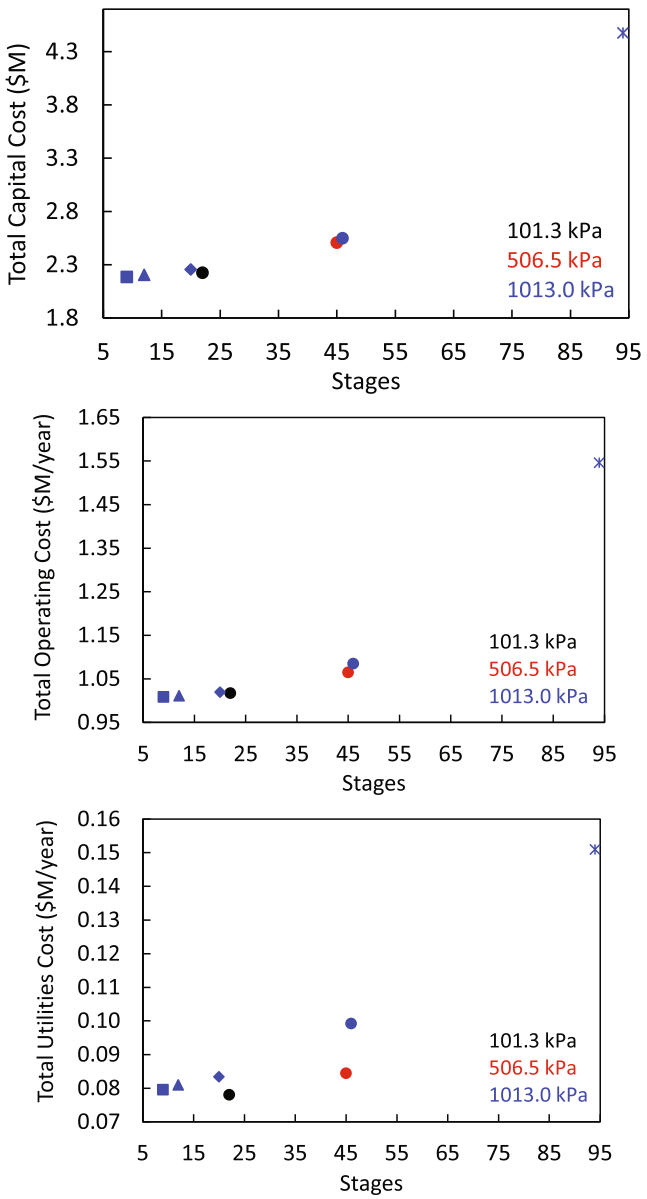


**FIGURE 11** Variation in costs with number of stages and column pressure: Case 1 (black circle), Case 2 (red circle), Case 3 (blue square), Case 4 (blue triangle), Case 5 (blue diamond), Case 6 (blue circle), and Case 7 (blue asterisk).

result, the composition of MeOH in the distillation and the composition of CPME in the bottom product were found to be almost identical. However, there is a significant difference in the molecular weight, which means that the feed stage would not be exactly in the middle but rather lower than the middle part to achieve an equal molar split. The column pressure remains the same for cases 3–7 at 1013.0 kPa. Since a high product quality ranging from 90.0% to 99.0% is desired, the required number of stages increases from 9 to 94 stages.

Similarly, the optimal reflux ratio demonstrates an upward trend, with values of 0.60, 0.65, 0.75, 1.70, and 5.00, respectively. Case 7 holds a special position due to its remarkably high product quality of 99.0%. As a result, our preliminary simulation estimates indicate a need for approximately 126 stages to achieve this exceptional quality. However, by increasing the operating reflux ratio, it was possible to decrease the stage requirement by around 25%. This is the reason why the reflux ratio of Case 7 stands out (at a slightly higher value of reflux) among the other cases. A comprehensive summary of all simulation parameters and design specifications can be found in Table 10.

The capital and operating costs for each case were evaluated using Aspen Plus Economic Analyzer. This evaluation process involved considering essential details, including plant parameters and utilities cost, which are documented in Tables 11 and 12, respectively. Additionally, Table 13 presents the normalized cost per kmol of CPME. Total capital cost, operating cost, and utility cost increase with the number of stages and reflux ratio, irrespective of column pressure. The effect of column pressure can be observed in utility cost: For lower column pressure, the utility cost is significantly lower (see Figure 11).

## 5 | CONCLUSION

The VLE data for the binary system of CPME + MeOH were determined experimentally in the isobaric pressure range of 60.0–101.3 kPa using an ebulliometer. $G^E$-based models were utilized to model these data, with the order of the best performing model in terms of fitting found to be: *Wilson* > *UNIQUAC* > *NRTL*. Azeotrope formation was observed in all pressure ranges from 60.0–101.3 kPa for $x_{CPME} = 0.093 - 0.075$. The Wilson model indicated a decrease in azeotrope composition and its disappearance at 1013.0 kPa.

The flash point of the binary mixture at 101.3 kPa, as well as the surface tension, relative Gibbs adsorption, and thickness of the surface layer at 298.15 K, were estimated using the Wilson model. The surface properties indicated a greater tendency for mixing rather than adsorption near the pure end of CPME. Additionally, a distillation column was designed for separation at pressures of 101.3, 506.5, and 1013.0 kPa, targeting different purities in Aspen Plus. The economic evaluation predicted the highest total cost requirement of $20.41/kmol of CPME at a column pressure of 1013.0 kPa and a CPME purity of 99.0%, while the least total cost requirement was projected to be $13.60/kmol of CPME at a column pressure of 1013.0 kPa and a CPME purity of 95.0%.

## AUTHOR CONTRIBUTIONS

**Kedar Joshi:** writing – original draft; methodology; conceptualization; investigation; formal analysis. **Vyomesh M. Parsana:** writing – review and editing; conceptualization; validation; funding acquisition; supervision; methodology; investigation. **Priyank Khirsariya:** data curation; visualization; investigation. **Mahinder Ramdin:** software; resources; writing – review and editing. **Thijs J. H. Vlugt:** writing – review and editing; supervision.

## ACKNOWLEDGMENTS

The authors acknowledge the financial support provided by the GTU RPS-MRP grant (GTU/IQAC/RPS-MRP/Sanction Letter/2024/3064) and infrastructural support provided by V.V.P. Engineering College, Rajkot.

## DATA AVAILABILITY STATEMENT

Data to support the findings of this work are provided in the Supporting Information. Data to produce Figure 1 is provided in Table 3. Data to produce Figure 2 is provided in Table S1. Data to produce Figures 3 and 4 are provided in Tables S2, S3, and S4. Data to produce Figure 5 are provided in Table S5. Data to produce Figures 6 and 7 is provided in Table 9. Data to produce Figure 9 is provided in Table S6. Data to produce Figure 10 is provided in Table S7. Data to produce Figure 11 is provided in Table S8.

## ORCID

*Kedar Joshi* https://orcid.org/0000-0002-4993-2189
*Vyomesh M. Parsana* https://orcid.org/0000-0002-7473-1354
*Priyank Khirsariya* https://orcid.org/0000-0002-4911-9673
*Mahinder Ramdin* https://orcid.org/0000-0002-8476-7035
*Thijs J. H. Vlugt* https://orcid.org/0000-0003-3059-8712

## REFERENCES

1. Watanabe K, Yamagiwa N, Torisawa Y. Cyclopentyl methyl ether as a new and alternative process solvent. *Org Process Res Dev*. 2007;11:251-258.
2. Watanabe K. The toxicological assessment of cyclopentyl methyl ether (CPME) as a green solvent. *Molecules*. 2013;18:3183-3194.
3. Henderson RK, Jiménez-González C, Constable DJ, et al. Expanding GSK's solvent selection guide–embedding sustainability into solvent selection starting at medicinal chemistry. *Green Chem*. 2011;13:854-862.
4. Zhang H. Measurements and comparative study of ternary liquid–liquid equilibria for water+ acrylic acid+ cyclopentyl methyl ether at (293.15, 303.15, and 313.15) K and 100.249 kPa. *J Chem Eng Data*. 2015;60:1371-1376.
5. Zhang H. Liquid–liquid phase equilibria of the quaternary system water (1)+ acrylic acid (2)+ acetic acid (3)+ cyclopentyl methyl ether (4): measurement, correlation, and comparative study. *Fluid Phase Equilib*. 2015;403:23-29.
6. Kin I, Ohta G, Teraishi K, Watanabe K. Process for production of cycloalkyl alkyl ethers. 2011 US Patent 8,017,813.
7. Jeong WJ, Cho H-k, Lim JS. Vapor–liquid equilibria for the binary mixtures of methanol+ cyclopentyl methyl ether (CPME). *Korean J Chem Eng*. 2016;33:2961-2967.
8. Poor HM, Sadrameli S. Calculation and prediction of binary mixture flash point using correlative and predictive local composition models. *Fluid Phase Equilib*. 2017;440:95-102.

9. Rafati A, Bagheri A, Khanchi A, Ghasemian E, Najafi M. Cyclopentyl methyl ether as a new and alternative process solvent. *J Colloid Interface Sci*. 2011;355:252-258.
10. Van Ness HC. Thermodynamics in the treatment of (vapor + liquid) equilibria. *J Chem Thermodyn*. 1995;27:113-134.
11. Olson JD. Measurement of vapor-liquid equilibria by ebulliometry. *Fluid Phase Equilib*. 1989;52:209-218.
12. Wisniak J, Ortega J, Fernández L. A fresh look at the thermodynamic consistency of vapour-liquid equilibria data. *J Chem Thermodyn*. 2017;105:385-395.
13. Parsana VM, Parikh S, Ziniya K, et al. Isobaric vapor–liquid equilibrium data for tetrahydrofuran + acetic acid and tetrahydrofuran + trichloroethylene mixtures. *J Chem Eng Data*. 2023;68:349-357.
14. Wilson GM, Vapor–Liquid Equilibrium XI. A new expression for the excess free energy of mixing. *J Am Chem Soc*. 1964;86:127-130.
15. Renon H, Prausnitz JM. Local compositions in thermodynamic excess functions for liquid mixtures. *AIChE J*. 1968;14:135-144.
16. Abrams DS, Prausnitz JM. Statistical thermodynamics of liquid mixtures: a new expression for the excess Gibbs energy of partly or completely miscible systems. *AIChE J*. 1975;21:116-128.
17. Parsana, VM, Parekh, U, Dabke, SP, et al. Isobaric vapor–liquid equilibrium data of binary systems containing 2-ethoxyethanol, 2-ethoxyethyl acetate, and toluene. *J Chem Eng Data*. 2020;65:4798-4804.
18. Parsana VM, Parikh SP. Isobaric vapour–liquid equilibrium data measurement for a binary system of green solvent 2-methyltetrahydrofuran and acetic acid at 101.3kPa. *Arab J Sci Eng*. 2019;44:5371-5379.
19. Laitinen AT, Parsana VM, Jauhiainen O, et al. Liquid–liquid extraction of formic acid with 2-methyltetrahydrofuran: experiments, process modeling, and economics. *Ind Eng Chem Res*. 2021;60:5588-5599.
20. Khirsariya P, Parsana V, Joshi K. Computation of isobaric vapor–liquid equilibrium (VLE) data of methyl tert-butyl ether (MTBE) + acetic acid (AA) system. *Phys Chem Res*. 2024;12:745-752.
21. Khirsariya P, Parsana VM, Joshi K. Measurement & correlation of isobaric vapor–liquid equilibrium (VLE) data of methyl tert-butyl ether (MTBE) + acetic acid (AA) system. *Chem Data Collect*. 2024;51:101134.
22. Wei I, Rowley R. A local composition model for multicomponent liquid mixture shear viscosity. *Chem Eng Sci*. 1985;40:401-408.
23. Glasstone S, Laidler KJ, Eyring H. The theory of rate processes: the kinetics of chemical reactions, viscosity, diffusion and electrochemical phenomena. 1941.
24. Novak LT. Entity–based Eyring–NRTL viscosity model for mixtures containing oils and bitumens. *Ind Eng Chem Res*. 2006;45:7329-7335.
25. Sprow FB, Prausnitz JM. Surface thermodynamics of liquid mixtures. *Can J Chem Eng*. 1967;45:25-28.
26. Abroodi M, Bagheri A, Razavizadeh BM. Investigation of surface tension and surface properties of alkanolamine–alcohol mixtures at T =313.15K and P = 90.6kPa. *J Mol Liq*. 2019;287:110924.
27. Mousavi NS, Romero-Martínez A, Ramírez-Verduzco LF. Predicting the surface tension of mixtures of fatty acid ethyl esters and biodiesel fuels using UNIFAC activity coefficients. *Fluid Phase Equilib*. 2020;507:112430.
28. Suarez JT, Torres-Marchal C, Rasmussen P. Prediction of surface tensions of nonelectrolyte solutions. *Chem Eng Sci*. 1989;44:782-785.
29. Peng D-Y, Robinson DB. A new two–constant equation of state. *Ind Eng Chem Fundam*. 1976;15:59-64.
30. Michelsen ML. A method for incorporating excess Gibbs energy models in equations of state. *Fluid Phase Equilib*. 1990;60:47-58.
31. Mejía A, Segura H, Vega LF, Wisniak J. Simultaneous prediction of interfacial tension and phase equilibria in binary mixtures: an approach based on cubic equations of state with improved mixing rules. *Fluid Phase Equilib*. 2005;227:225-238.
32. Mejía A, Segura H, Cartes M, Pérez-Correa JR. Experimental determination and theoretical modeling of the vapor–liquid equilibrium and surface tensions of hexane+tetrahydro-2H-pyran. *Fluid Phase Equilib*. 2012;316:55-65.
33. Mejía A, Segura H, Cartes M. Experimental determination and theoretical prediction of the vapor–liquid equilibrium and interfacial tensions of the system methyl-tert-butyl ether+2,5-dimethylfuran. *Fuel*. 2014;116:183-190.
34. Kleinheins J, Shardt N, El Haber M, et al. Surface tension models for binary aqueous solutions: a review and intercomparison. *Phys Chem Chem Phys*. 2023;25:11055-11074.
35. Wypych G. *Databook of Green Solvents*. Elsevier Science; 2019.
36. Yang C, Lai H, Liu Z, Ma P. Densities and viscosities of diethyl carbonate + toluene, + methanol, and + 2-propanol from (293.15 to 363.15) K. *J Chem Eng Data*. 2006;51:584-589.
37. Parsana V, Parikh S. Vapor–liquid equilibrium data prediction by advanced group contribution methods for a binary system of cyclopentyl methyl ether and acetic acid at atmospheric pressure. *Res J Chem Sci*. 2015;5:64-72.
38. Camacho J, Díez E, Díaz I, Ovejero G. Vapor–liquid equilibrium at p/kPa = 101.3 of the binary mixtures of ethenyl acetate with methanol and Butan-1-ol. *J Chem Eng Data*. 2012;57:3198-3202.
39. Poling B, Prausnitz J, O'Connell J. *The Properties of Gases and Liquids 5E*. McGraw Hill Professional. McGraw Hill LLC; 2000.
40. Turton R, Shaeiwitz J, Bhattacharyya D, Whiting W. *Analysis, Synthesis, and Design of Chemical Processes*. Prentice-Hall international Series in the Physical and Chemical Engineering Sciences. Prentice Hall; 2018.


## SUPPORTING INFORMATION

Additional supporting information can be found online in the Supporting Information section at the end of this article.

**How to cite this article:** Joshi K, Parsana VM, Khirsariya P, Ramdin M, Vlugt TJH. Vapor-liquid equilibrium, thermodynamic properties, process simulation and economic evaluation of CPME and methanol system. *AIChE J*. 2025; e18877. doi:10.1002/aic.18877